



1 **Hydrological control of large hurricane-induced lahars: evidences from rainfall,**
2 **seismic and video monitoring**

3 Lucia Capra¹, Velio Coviello¹, Lorenzo Borselli², Víctor-Hugo Márquez-Ramírez¹, Raul
4 Arámbula-Mendoza³

5 ¹ *Centro de Geociencias, Universidad Nacional Autónoma de México (UNAM), Campus*
6 *Juriquilla, Queretaro, México*

7 ² *Instituto de Geología, Universidad Autónoma de San Luis Potosí, San Luis Potosí,*
8 *México*

9 ³ *Centro Universitario de Estudios e Investigaciones en Vulcanología (CUEIV),*
10 *Universidad de Colima, Colima, México.*

11

12 **Abstract**

13 The Volcán de Colima, one of the most active volcanoes in Mexico, is commonly affected
14 by tropical rains related to hurricanes that form over the Pacific Ocean. In 2001, 2013 and
15 2016 hurricanes Jova, Manuel and Patricia, respectively, promoted tropical storms that
16 accumulated up to 400 mm of rain in 36 hrs, with maximum intensities of 50 mm/hrs.
17 Effects were devastating, with the formation of multiple lahars along La Lumbre and
18 Montegrande ravines, which are the most active channels in sediment delivery on the S-SW
19 flank of the volcano. Deep erosion along the river channels and several landslides at their
20 side were observed, and damages to bridges and paved roads for the arrival of block-rich
21 fronts resulted in the distal reach of the ravines. Based on data from real-time monitoring
22 (including images, seismic records and rainfall data), the temporal sequence of these events
23 is reconstructed and analyzed with respect to the rainfall characteristics and the
24 hydrological response of the watersheds based on rainfall/infiltration numerical simulation.



25 For the studied events, lahars occurred after 5-6 hours since rainfall started, lasted several
26 hours and were characterized by several pulses with block-rich fronts and a maximum flow
27 discharge of $900 \text{ m}^3/\text{s}$. Rainfall/infiltration simulations were performed with the Flo-2D
28 code using the SCS-Curve number infiltration model. Results show different behaviors for
29 the arrival times of the first lahar pulses that correlate with the catchment's peak discharge
30 for La Lumbre ravine and with the peaks in rainfall intensity for Montegrande ravine. This
31 different behavior is strictly related to the area and shape of these two watersheds.
32 Nevertheless, for all the analyzed cases, the largest lahar pulse always corresponds with the
33 last one and correlates with the maximum peak discharge of these catchments. Data here
34 presented show that main pulses within a lahar are not randomly distributed in time, and
35 they can be correlated with rainfall peak intensity and/or watershed discharge, depending
36 on the watershed area and shape. This outcome has important implications for hazard
37 assessment during extreme hydro-meteorological events since it could help in real-time
38 alert. A stormwater was here designed based on the rainfall time distribution of hurricanes
39 Manuel and Patricia and, in case on available weather forecasts, it can be used to run
40 simulations prior to the event, and have an estimation of the time arrivals of main pulses,
41 usually characterized by block-rich fronts that are responsible of damage to infrastructures
42 and loss of goods and lives.

43

44 **Keywords:** *lahar, hurricane, rainfall/infiltration simulation, Volcán de Colima, Mexico.*

45

46 **1. Introduction**



47 In past recent years hurricanes have had catastrophic effects on volcanoes of the
48 world triggering lahars (sediment-water gravity-driven flows on volcanoes). One of the
49 most recent episode is represented by the 2009 Hurricane Ida in El Salvador that caused
50 several landslides and debris flows from the Chichontepec volcano, killing 124 people, or
51 by the 1998 Hurricane Mitch that triggered the collapse of a small portion of the inactive
52 Casita volcano, originating a landslide that suddenly transformed into a lahar that
53 devastated several towns and killed 2000 people (Van Wyk Vries et al., 2000; Scott et al.,
54 2005). A similar event was observed in 2005 when tropical storm Stan triggered landslides
55 and debris flows from the Toliman Volcano (Guatemala), causing more than 400 fatalities
56 at Panabaj community (Sheridan et al., 2007). Other examples can be found at the
57 volcanoes Pinatubo (Philippines), Merapi and Semeru (Indonesia), Soufrière (Montserrat),
58 Mt. Ruapehu (New Zealand), where tropical storms and heavy rainfall seasons have
59 triggered high-frequency lahar events (Umbal and Rodolfo, 1996; Cronin et al., 1997;
60 Lavigne et al., 2000; Lavigne and Thouret, 2002; Barclay et al., 2007; Dumaisnil et al.,
61 2010; Doyle et al., 2010, de Bélizal et al., 2013).

62 Volcán de Colima ($19^{\circ}31'N$, $103^{\circ}37' W$, 3860 m a.s.l., Fig. 1), one of the most
63 active volcanoes in Mexico, is periodically exposed to intense seasonal rainfalls that are
64 responsible for the occurrence of lahars from June to late October (Davila et al., 2007;
65 Capra et al., 2010). Rain-triggered lahars represent a very common process during the rainy
66 season (June-October) at Volcán de Colima (Davila et al., 2007; Capra et al., 2010;
67 Vazquez et al., 2016a). They usually affect areas as much as 15 km from the summit of the
68 volcano, with resulting damage to bridges and electric power towers (Capra et al., 2010),
69 and are more frequent just after eruptive episodes such as dome collapse emplacing block-



70 and-ash flow deposits (Davila et al., 2007; Vázquez et al., 2016b). Several hurricanes
71 commonly hit the Pacific Coast each year and proceed inland as tropical rainstorm reaching
72 the Volcán de Colima area. In particular, on 2011, 2013 and 2015 Jova, Manuel and
73 Patricia hurricane respectively triggered long-lasting lahars along main ravines, causing
74 several damages on roads and bridges, leaven uncommunicated for few days several
75 communities in a radius of 15 km from the volcano.

76 Previous work (Davila et al., 2007; Capra et al., 2010) analyzed the lahars frequency
77 at Volcán de Colima in relation with the eruptive activity and the characteristics of
78 rainfalls. Lahars are more frequent at the beginning of the rains season, during short (< 1
79 hour) stationary rainfalls, with variable rainfall intensities and with only 10 mm of
80 accumulated rainfall. This behavior has been attributed to a hydrophobic effect of soils on
81 the volcano slope (Capra et al., 2010). In contrast, in the late rain season, when tropical
82 rainstorms are common, lahars are triggered depending on the 3-day antecedent rainfall and
83 with intensities that increase as the total rainfall amount increases (Capra et al., 2010). The
84 lahars record used for these previous studies was only based on seismic data. Since 2011 a
85 visual monitoring system have been installed on Montegrande and La Lumbre ravines
86 (Figure 1), based on which a quantitative characterization of some events (i.e type of flow,
87 velocity, flow discharge, flow fluctuation) have been possible (i.e. Vázquez et al., 2016a;
88 Coviello et al., under revision). The aim of the present paper is to better understand the
89 lahars initiation processes and their dynamical behavior, especially during hurricane events,
90 when more damages have been observed on inhabited area. In particular, the arrival time of
91 main lahar's front/surge at the monitoring stations is here analyzed with respect to the
92 rainfall characteristics (rain accumulation and intensity) in relation with the hydrological



93 response of the watersheds based on rainfall/infiltration numerical simulation. The
94 occurrence of discrete surges within lahars have been attributed to spatially and temporally
95 distributed lahar sources, temporary damming, progressive entrainment of bed material or
96 change in slope angle (i.e. Iverson 1997; Marchi et al. 2002; Takahashi 2007; Zanuttigh and
97 Lamberti 2007; Doyle et al., 2010; Kean et al., 2013). Without excluding previous models,
98 data here presented shows that main pulses within a lahar are not randomly distributed in
99 time, and they can be correlated with rainfall peak intensity and/or watershed discharge,
100 depending on the watershed shape and hydrophobic behavior subject to the antecedent soil
101 moisture. The lahars triggered by the hurricanes Jova, Manuel and Patricia are here used as
102 they correspond with the best documented events occurred during past years, and they will
103 be also compared with an extraordinary hydrometeorological event occurred at the begin of
104 the rain season (11 June, 2013) to better show the drastic change on lahar initiation due to
105 the hydrophobic effect of soils at Volcán de Colima. Based on rainfall distribution over
106 time for the analyzed events, a stormwater is here designed, which can be used to run
107 simulations prior to an event to have an estimation of the time arrivals of main pulses when
108 weather forecast is available. The data here presented have important implication for hazard
109 assessment during extreme hydrometeorological events as a complementary tool of an early
110 warning system.

111

112 2. Methods and data

113 2.1. La Lumbre and Montegrande watersheds



114 The source area of lahars at Volcán de Colima corresponds to the uppermost unvegetated
115 portion of the cone (Fig. 1 and 2a), with slopes between 35° and 20°, that also corresponds
116 with an area of high connectivity, being prone to rills formation and erosive processes
117 (Ortiz et al., 2017). The channels along main ravines have slopes from 15° up to 4° in the
118 more distal reach, they are flanked by densely vegetated terraces, up to 15 m high in
119 average, that consist of debris avalanche and pyroclastic deposits from past eruptions (Figs.
120 2b and c) (Cortes et al., 2010; Roverato et al., 2011). Seven major watersheds from 2 to 14
121 km² feed the main ravines draining from the volcano on the southern side (Fig. 1). La
122 Lumbre is the largest watershed, with a total area of 14 km², and Montegrande is in average
123 with the other catchments, with an area of 2 km² (Fig. 1). Beside the difference in total
124 area, the Montegrande and La Lumbre watersheds are quite different in geometry.
125 Montegrande catchment is elongated, with a maximum width of 800 m, 300 m in average.
126 In contrast, the proximal portion of the La Lumbre catchment includes all the NW slope of
127 the cone, to then extent to a more elongated shape towards SW, being up to 1500 m in
128 width. These differences in area and shape can be correlated with a different response in
129 water discharge under a rainfall event. In circular drainages, as the proximal portion of the
130 La Lumbre watershed, all points are quite equidistant from the main river so all the
131 precipitation reaches the river at the same time, concentrating a large volume of water. In
132 contrast, in a more elongate basin, lateral drainages quickly drain water on the main
133 channel at different points but with a lower total discharge. The Gravelius's index K_g
134 (Bendjoudi and Hubert 2002), which is defined as the relation between the perimeter of the
135 watershed (P) and that of a circle having a surface equal to that of a watershed (A):

$$K_g = \frac{P}{2\sqrt{\pi A}}$$



136 is here estimated for Montegrando watershed and for the upper, circular portion of La
137 Lumbre watershed obtaining values of 1.7 and 1.1 respectively. The lower the value, the
138 more regular the basin's perimeter and the more prone it is to present high runoff peaks.
139 Based on these considerations, at La Lumbre watershed a larger volume of water
140 concentrates along the main channel because of its larger surface and circular shape, but
141 after a larger period of time respect to Montegrando ravine, where a minor volume of water
142 quickly reaches the main drainage.

143

144 **2.2 Lahar Monitoring at Volcán de Colima**

145 In 2007, a monitoring program was implemented at Volcán de Colima. At the beginning,
146 two rain gauges were installed to study lahar initiation (AR and PH sites, Figure 1) and
147 lahar propagation was detected by the broadband seismic stations of RESCO, the
148 seismological network of Colima University (Davila et al., 2007; Zobin et al., 2009; Capra
149 et al., 2010). Afterwards, two monitoring station specifically designed for studying lahar
150 activity were installed, in 2011 at the Montegrando ravine and in 2014 at La Lumbre ravine
151 (MSMg and MSL respectively, Figure 1). Both stations consist of a 12 m-high tower with a
152 directional antenna transmitting data in real time to RESCO facilities, a camcorder
153 recording images each 2-4 secs with a 704 x 480 pixels in resolution, a rain gauge coupled
154 with a soil moisture sensor, and a 10 Hz geophone (Vázquez et al., 2016a; Coviello et al.,
155 under revision). The rain gauge (HOBO RG3) records rain accumulation at one-minute
156 intervals. At Montegrando ravine seismic data are also obtained from a 3 component Guralp



157 CMG-6TD broadband seismometer installed at 500 m upstream from the monitoring site,
158 sampling at 100 Hz (BB-RESCO, Figure 1).

159 Montegrande station detected lahars occurred during 2011 Jova and 2013 Manuel events,
160 and lahars triggered during the 2015 Hurricane Patricia were only recorded by La Lumbre
161 station (Table 1). In fact, in 2011 only MgMS site was operating (as the BB-RESCO
162 station), and recorded the seismic signal of the lahar associated to Jova and Manuel. No
163 images are available since both events occurred during the night. The LMS station starts to
164 operate at the end of 2013 and was able to record the lahars associated to Hurricane Patricia
165 along the La Lumbre ravine (images and geophone data). In contrast, in 2015 the MgMS
166 was destroyed by pyroclastic flows during the 10-11 explosive activity, and in October
167 2015 the new station was still under construction. Only few pictures were acquired and they
168 are of low quality because of the abundant steam coming from the hot lahars since they
169 originated from the remobilization of fresh pyroclastic flow deposits (Capra et al., 2016).
170 The 11 June 2013 event was perfectly captured by the camera installed at the MgMS site
171 and the BB-RESCO recorded its seismic signal.

172 The seismic signal is here analyzed to detect the arrival of main flow fronts and discharge
173 variation. For this, only the amplitude of the signal is considered, which can be correlated
174 with the variation in the maximum peak flow discharge (Doyle et al., 2010; Vázquez et al.,
175 2016a). The seismic record is here compared with the available images to identify the main
176 changes in dynamic of the detected lahars. All the lahars here analyzed correspond to multi-
177 pulses events as classified by Vazquez et al. (2016a); they consist of long lasting lahars
178 presenting several pulses each one characterized by a block-rich front followed by the main
179 body and dilute tail showing continuous changes in flow discharges. A detailed seismic



180 description of these types of lahars is available in Vázquez et al. (2016a), here we focus on
181 the number of main flow peaks and their arrival times (Table 2).

182

183 **2.3. The hydrometeorological events**

184 Hurricane Jova formed over the Pacific Ocean, hit the Pacific coast on October 12, 2011, as
185 a category 2, and traveled inland toward Volcán de Colima. The hurricane arrived as a
186 tropical storm at the town of Coquimatlán, just 10 km SW of the city of Colima with winds
187 up to 140 km/h, and 240 mm of rain over 24 h (Fig. 3a). Severe damage was registered in
188 inhabited area, including the city of Colima where floods damaged roads, bridges and
189 buildings.

190 The 2013 Hurricane Manuel of category 1, hit the pacific coast during national holidays
191 (Fiestas Patria) causing several damage to mountainous region in Guerrero state, triggering
192 several landslides that caused up to 96 deaths and left several villages uncommunicated as
193 thousands of tourists trapped at Acapulco and Ixtapa international airports. At Volcan the
194 Colima rains started on September 15 and lasted for more than 30 hrs with more than 300
195 mm of accumulated rains (Fig. 3a).

196 The 2015 Hurricane Patricia was considered as the strongest hurricane on record to affect
197 Mexico. The system starts to develop on 18 October over the Pacific Ocean, strengthened
198 into a hurricane shortly after 00:00 GMT 22 October and early on 23 October it reached its
199 maximum category of 5. But late on the same day, the system rapidly lost its strength. It
200 landfalls around 23:00 GMT along the coast of the Mexican state of Jalisco near Playa
201 Cuixmala, about 60 km west-northwest of Manzanillo. On the morning of the 23 October,



202 2015 it continued to rapidly weaken as it moves on the Sierra Madre Occidental high
203 relieves. At Colima town, up to 400 mm of rains accumulated along 30 hours since the
204 morning of 23 October (Fig. 3a). Lahars along the Montegrande ravine were hot since they
205 originated from the erosion of pyroclastic flow deposits emplaced during the 10-11 July
206 2015 eruption. Sever damages affected the Colima town and the volcano surrounding. A
207 bridge along the interstate was destroyed leaving uncommunicated La Becerrara village and
208 interrupting the traffic between Colima and Jalisco states.

209 Patricia and Manuel rainfalls show a similar behavior, with a progressive rain accumulation
210 along 28-30 hrs; in contrast, during Hurricane Jova, 200 mm of rain accumulated in less
211 than 15 hrs reaching a total of 240 mm during the following 13 hrs (Fig. 3a). These
212 differences are more evident plotting the 10-min accumulated value normalized over the
213 total accumulated rainfall (Fig. 3b). Average rainfall intensities calculated over a 10-min
214 interval range from 32 mm/hrs to 37 mm/hrs for Manuel and Patricia events respectively
215 and up to 43 mm /hrs for the Hurricane Jova (Table 2). Finally rainfall values were
216 calculated at selected intervals (15 m, 30 m, 45 mm, 1, 3, 6, 12, 18, 24, 28 hr) to design
217 possible storm rainfall distributions based on tropical rains associated to hurricanes
218 recorded so far at Colima Volcano (Table 2). Considering the similar behavior of the
219 Manuel and Patricia rainfalls, a stormwater can be designed considering their average
220 values (Fig. 3c) (i.e. NRCS, 2008), based on which a forecast analysis can be performed, as
221 will be discussed below.

222

223 **2.4. Rainfall simulations**



224 To better understand the lahar behavior and duration during extreme hydrometeorological
225 event at Volcán de Colima, rainfall simulations were performed with Flo-2D code (O'Brian
226 et al., 1993). The Flo-2D code routes the overland flow as discretized shallow sheet flow
227 using the Green-Ampt or the SCS Curve number (or combined) infiltration models. For the
228 present work the SCS Curve Number (SCS-CN, i.e. Mishra and Singh, 2003) was selected.
229 With this model, the volume of water runoff produced for the simulated precipitation is
230 estimated through a single parameter that summarizes the influence of both the superficial
231 aspects and deep soil, including the saturated hydraulic conductivity, type of land use, and
232 humidity before the precipitation event. A similar approach was already used for modeling
233 debris flow initiation mechanisms (i.e. Gentile et al., 2006; Llanes et al., 2015). To apply
234 the SCS-CN model, it is necessary to classify the soil in one of four groups, each
235 identifying a different potential runoff generation (A, B, C, D; USDA-NRCS 2007). The
236 watershed of La Lumbre and Montegrande ravines were subdivided in two main zone: the
237 unvegetated upper cone and the main channel that consist of unconsolidated pyroclastic
238 material with large boulders imbedded in sandy to silty matrix, and the vegetated lateral
239 terraces. Lateral terraces consist of old pyroclastic sequences, with incipient soils and
240 vegetated with pine trees and sparse brushes, with soils that show a hydrophobic behavior
241 at the beginning of the rain season (Capra et al., 2010). In-situ infiltration tests were also
242 performed based on which values of saturated conductivity were obtained in the range of 50
243 mm/h (nude soil) to 100 mm/h (vegetated) (Ortiz, 2017). Based on these observations, soils
244 were classified between group A and B (Bartolini and Borselli, 2009). Curve Numbers for
245 the vegetated terraces and for the nude soils were estimated in 75 and 80 respectively (in
246 wet season, Hawkins et al., 1985; Ferrer-Julia et al. 2003). To perform simulation with the
247 FLO-2D code, two polygons were traced to delimit the un-vegetated portion of the cone



248 from the vegetated area of the watershed, and at each polygon the relative CN value was
249 assigned. The simulated rain corresponds with the cumulative value calculated at 10
250 minutes interval (Fig. 3b). At the apex of each watershed a barrier of outflow points were
251 defined to obtain the total values of the watershed discharge. The simulation was performed
252 with a 20-m digital elevation model.

253

254 **3. Results**

255 During the Jova hurricane, lahars started in Montegrande ravine early in the morning of 12
256 October, 2011, around 07:20 GMT (here after all time is in GMT), after approximately 40
257 % of the total rain (240 mm) accumulated (Fig. 4a). The event lasted more than 4 hours,
258 and three main peaks in amplitude can be detected in the seismic signal (Fig. 4a). In
259 particular, the first two peaks are similar in amplitude (0.015 cm/s), separated by more than
260 2 hours of signal fluctuation. After less than one hour from the second peak, a single,
261 discrete pulse can be recognized (0.05 cm/s in amplitude), followed by a “train” of low-
262 amplitude seismic peaks that lasted for more than an hour.

263 Along the same ravine, an extreme event was recorded on 11 June, 2013. This event
264 corresponds to an extraordinary episode and is here introduced to better discuss the
265 hydrological response of the Montegrande ravine. It represents an unusual event at the
266 beginning of the rainy season, considering the total accumulated rainfall of 120 mm in less
267 than 3 hrs (Table 2), with maximum pick intensity up to 140 mm/hr (Fig. 4b). Based on the
268 seismic record and the still images of the event, this lahar was previously characterized as a
269 multi-pulse flow, with three main blocks-rich fronts (I, II and IV, Fig. 4c), with similar



270 amplitudes (0.015-0.025 cm/s), followed by a main flow body consisting of a homogenous
271 mixture of water and sediments (with a sediment concentration at the transition between a
272 debris flow and an hyperconcentrated flow) (III, Fig. 4c) (Vazquez et al. 2016a). The last,
273 more energetic pulse (0.042 cm/s) was accompanied by a water-rich frontal surge that was
274 able to reach the lens of the camera (IV, Fig. 4c). Comparing the Jova and the 2013 event
275 seismic records it is possible to note that in both events, the largest pulse corresponds with
276 the last one. Flow discharge was estimated for the 2013 event, with a maximum of 120 m³/s
277 value for the largest pulses (IV, Figure 4b) (Vazquez et al., 2016a). For the Jova event, the
278 only visual data available are the images of the channel the day before and the day after the
279 event, where a deep erosion of the channel is visible (Fig. 5), but comparing its seismic
280 signal with the 2013 lahar, and based on the classification criterion established for lahars at
281 Volcán de Colima (Vazquez et al., 2016a) each main peak corresponds to the arrival of
282 flow surges or to block-rich fronts followed by the body of the flow. Fluctuation in seismic
283 energy along the vertical component reflects variation in flow discharge.

284 The lahar recorded during the Hurricane Manuel along the Montegrande ravine shows a
285 similar behavior as described for the Jova event (Fig. 6). As the event occurred during the
286 night no images are available. Based on the seismic record from the BB-RESCO, lahars
287 started around 03:00, and lasted for seven hours. The event was characterized by five main
288 pulses, which amplitude increases with time (0.012-0.025 cm/s), being the last one the
289 larger in magnitude (0.04 cm/s). Based on the amplitude values, the first two peaks
290 correspond to precursory dilute flow waves followed by the three main pulses with block-
291 rich fronts (I, II and III, Fig 6).



292 For the Hurricane Patricia seismic data (from the geophone) and still images were recorded
293 at the La Lumbre monitoring station. Based on these data, at approximately 21:22 a slurry
294 flow is detected on the main channel (Fig. 7a). First pulses of hyperconcentrated flows were
295 detected around 01:30 (24 October) which progressively increased in flow discharge and
296 sediment concentration. Several front waves were observed during flooding (I and II, Fig.
297 7b) for which an average flow discharge of 80-100 m³/sec was estimated, and two main
298 pulses arrived at 04:30 and 05:00, with 6 m-depth block-rich fronts and maximum flow
299 discharge of 900 m³/sec (III, IV, V and VI, Fig. 7b). At around 05:40 the seismic record
300 detected the arrival of a third pulse. Although no images were available, the amplitude of
301 the last pulse (0.07 cm/s) suggests it was larger than those previously described. As
302 observed for the three events recorded at Montegrande ravine, the largest pulse correspond
303 again with the last one.

304 The results of rainfall simulations are plotted as a normalized curve of the total discharge,
305 along with the normalized accumulated rainfall and its intensity (calculated over a 10-min
306 interval) (Fig. 8). In the same plot, the arrival time of the main lahar pulses here analyzed is
307 also indicated (red triangles, Fig. 8). By comparing watershed discharge with rainfall
308 intensity, a general correlation can be observed for the Montegrande basin during Jova and
309 Manuel hurricane, contrasting with the June 2013 event, where the simulation is not able to
310 reproduce watershed discharge during the first minutes of the event when most of rainfall is
311 accumulated and maximum rainfall intensities are detected. For la Lumbre watershed a
312 clear correlation between peak intensities and watershed discharge is not clearly
313 observable. If the arrival times of the main lahars' pulses are considered, the events
314 associated to the hurricanes Jova and Manuel along the Montegrande ravine show a similar



315 behavior. In both cases early slurry flows are detected after ~40% of the total rain is
316 accumulated. The main flow pulses better correlate with the highest rain intensity values,
317 which also correspond with maximum peaks in watershed discharge; the last, largest pulse
318 corresponds with the maximum peak discharge of the watershed. In contrast, for the
319 Patricia event, along the La Lumbre ravine, first slurry flows also starts after 40% or
320 rainfall accumulated, but main lahar pulses fit better with the peaks watershed discharge.
321 Finally, analyzing the simulation in the Montegrande ravine for the June 2013 event, it is
322 possible to observe a different behavior. The lahar starts as less than the 10% of rain is
323 accumulated, and the main lahar pulses perfectly correlate with the peak rainfall intensities,
324 and only the last largest pulse correlates with the watershed peak discharge.

325

326 **4. Discussion**

327 At present, several attempts to define lahar rainfall thresholds have been already carried out
328 for different volcanoes (i.e. Lavigne et al., 2000; van Westen and Daag, 2005 Barclay et al.,
329 2007), including Volcán de Colima (Capra et al., 2010). This study is mostly addressed to
330 better predict the lahar evolution during extraordinary hydrometeorological event as
331 hurricane, a common long-duration and large-scale rainfall phenomenon at tropical
332 latitudes. In particular, we are interested in predicting the arrival of block-rich fronts that
333 have caused several damages during past events. Based on the seismic and visual data
334 gathered from the events here analyzed, it is possible to evidence which are the key factors
335 in controlling the arrival of main lahars fronts. For Jova, Manuel and Patricia events, lahars
336 started after the 40% of total rain accumulated, and apparently the timing for the initial



337 pulses correlate well with the peaks of the rainfall intensity for the Montegrande ravine,
338 while for la Lumbre ravine they better match with the watershed discharge. Nevertheless
339 for all analyzed cases, the largest pulses correspond with the last ones and correlate with the
340 peak watershed discharge for all the analyzed examples. The observed difference between
341 Montegrande and La Lumbre ravines can be correlated with the different areas and shapes
342 of the two catchments. In fact, due to its elongated shape ($K_G = 1.7$) and small area ($A = 2$
343 km), the Montegrande watershed shows a quicker response between rainfall and discharge,
344 with a rapid water runoff that concentrated at different point along the main channel (Fig.
345 1b). This behavior is much clearer for the June 2013 event, which occurred at the beginning
346 of the rain season when soils on the lateral terraces of the ravines show a hydrophobic
347 behavior (Capra et al., 2010). The simulation is not able to reproduce any watershed
348 discharge at the beginning of the event, because the hydrophobic behavior of the soils
349 inhibits the infiltration and the water runoff quickly promotes lahar initiation. During this
350 event, the first lahar pulses perfectly match with the rainfall peak intensities (except for the
351 last major pulse), starting from the very beginning of the rainfall event. In contrast, La
352 Lumbre ravine has a wider, rounded upper watershed ($K_G = 1.1$; $A = 14 \text{ km}^2$) that is able to
353 concentrated a larger volume of water before to turn SW in the main channel where lateral
354 contribution can still increase water discharge. Even if rainfalls of hurricanes Manuel and
355 Patricia show a similar behavior (Fig. 3), the catchment response of La Lumbre is clearly
356 different with a pulsating behavior of lahars mainly controlled by the watershed discharge.
357 Nevertheless, for all the events here analyzed, the largest pulse corresponds with the last
358 one recorded and it correlates with the maximum watershed discharge, pointing to a strong
359 control of the catchments recharge in generating the largest and more destructive pulses.
360 Previous works correlated the occurrence of surges within a lahar to multiple sources, such



361 as lateral tributaries along the main channel (i.e. Doyle et al., 2010) or due to the failure of
362 temporary dams of large clasts in correspondence of an increase in rainfall intensity (Kean
363 et al., 2013). Lateral tributaries are absent in both Montegrande and La Lumbre channels
364 and, even if accumulation of clasts it is possible, no significant discontinuities of the
365 channel bed can be observed upstream the monitoring sites. Based on data here presented,
366 formation of pulses within a lahar is mostly controlled with the increase in water runoff that
367 at a critical discharge rate mobilize a large volume of sediment where large clasts
368 accumulate at its front. This is a well-documented mechanism (i.e. Iverson, 1997), but
369 based on the model here proposed, the discharge rate is controlled by the watershed
370 discharge that regulates the timing on the arrival of main pulses, depending on the rainfall
371 behavior and the watershed shape. Nevertheless, the last pulse always is the largest in
372 volume. This model is strictly related to migratory, long-duration and large-scale rainfall
373 events hitting tropical volcanoes such as the Volcán de Colima. In fact, during mesoscale
374 non-stationary rainfalls, typical at the beginning of the rainy season, lahars are usually
375 triggered at low accumulated rainfall values and controlled by rainfall intensity due to the
376 hydrophobic behavior of soils, and they usually consist of uni-pulse events with a single
377 block-rich front that last less than one hour (i.e. Vázquez et al., 2016b). In perspective, the
378 results here presented can be used to design an Early Warning System (EWS) for hurricane-
379 induced lahars, i.e. event triggered by long-duration and large-scale rainfalls. Most
380 common pre-event or advance-EWSs for debris flows are based on empirical correlations
381 between rainfall and debris flow occurrence (e.g., Keefer et al., 1987; Aleotti, 2004; Baum
382 and Godt, 2009). The instruments adopted for debris-flow advance warning are those
383 normally used for hydrometeorological monitoring and consist of telemetry networks of
384 rain gauges and/or weather radar. The typical way to represent these relations is identifying



385 critical rainfall thresholds for debris flow occurrence. The availability of both a large
386 catalogue of events and a reliable precipitation forecast that could give the predicted
387 amount of rainfall some hours in advance would allow the issue of an effective warning, at
388 least in predicting the arrival time of the main lahar pulses. In addition, instrumental
389 monitoring of in-channel processes can be used to validate a preliminary warning-condition
390 triggered by wheatear forecast and/or rainfall measurements.

391

392 **5. Conclusions**

393 Real time monitoring of lahars at Volcán de Colima volcanoes reveal that watershed
394 discharge is the key factor in controlling the arrival of main block-rich fronts during long-
395 lasting lahar triggered during tropical storms, and that the largest destructive pulses will
396 arrive after the initial surging. For the 2015 Hurricane Patricia event the weather forecast
397 predicted an estimated value for the total rainfall, as also the approximate time of its
398 landfall. Based on the deigned storm obtained with the time rainfall distribution of the
399 event here analyzed, it could have been possible to anticipate when lahars started along the
400 La Lumbre ravine, and the arrival time of main pulses. Along the other ravines, that show a
401 watershed similar to the Montegrande, it could have been possible to predict the arrival of
402 at least the largest pulse. This information coupled with the real time monitoring could be a
403 better tool for hazard assessment and risk mitigation. In fact, these findings can be used to
404 implement an advance warning system based on the monitoring of a hydrometeorological
405 process to issue a warning before a possible lahar is triggered.

406



407 **Acknowledgements.**

408 This work was supported by CONACyT projects 230 and 220786 granted to Lucia Capra
409 and by the postdoctoral fellowship of DGAPA (Programa de Becas Posdoctorales de la
410 UNAM) granted to Velio Coviello. Thanks to José Luis Ortiz and Sergio Rodríguez, from
411 the Centro de Prevención de Desastres (CENAPRED), who set up the instrumentation on
412 the Montegrande monitoring site.

413

414 **References**

415 Aleotti P (2004) A warning system for rainfall-induced shallow failures. *Eng. Geol.* 73(3-
416 4): 247–265.

417 Barclay J, Alexander J, Susnik L (2007) Rainfall-induced lahars in the Belham valley,
418 Monserrat, West Indies. *Journal of the Geological Society of London* 164: 815-827.

419 Bartolini D, Borselli L (2009) Evaluation of the HydrologicSoil Group (HSG) with the
420 Procedure SCS Curve Number. In: *Manual of Methods for Soil and Land Evaluation*,

421 Edoardo A, Costantini C (ed), Science Publisher Inc., 600 pages. ISBN 978-1-57808-571-2

422 Baum R L, Godt JW (2009) Early warning of rainfall-induced shallow landslides and debris
423 flows in the USA. *Landslides* 7(3): 259–272.

424 Bendjoudi H, Hubert P (2002) Le coefficient de Gravélius : analyse critique d'un indice de
425 forme des bassins versants. *J. Sci. Hydrol.* 47: 921–930.



- 426 Capra L, Borselli L, Varley N, Norini G, Gavilanes-Ruiz JC Sarocchi D, Caballero L
427 (2010) Rainfall-triggered lahars at Volcán de Colima, Mexico: surface hydro-repellency as
428 initiation process. *Journal of Volcanology and Geothermal Research* 189(1-2): 105-117.
- 429 Cortes A, Macias JL, Capra L, Garduño-Monroy VH (2010) Sector collapse of the SW
430 flank of Volcán de Colima, México. The 3600 yr BP La Lumbre-Los Ganchos debris
431 avalanche and associated debris flows. *Journal of Volcanology and Geothermal Research*
432 197: 52-66.
- 433 Coviello V, Capra L, Vázquez R, Marquez-Ramirez V, under revision. Seismic
434 characterization of hyperconcentrated flows in volcanic environment. *Earth Surface*
435 *Processes and Landforms*.
- 436 Cronin SJ, Hodgson KA, Neall VE, Palmer AS, Lecointre JA (1997) 1995 Ruapehu lahars
437 in relation to the late Holocene lahars of Whangaehu River, New Zealand. *New Zealand*
438 *Journal of Geology and Geophysics* 40: 507-520.
- 439 Davila N, Capra L, Gavilanes JC, Varley N, Norini G (2007) Recent lahars at Volcán de
440 Colima (Mexico): drainage variation and spectral classification. *Journal of Volcanology*
441 *and Geothermal Research* 165: 127-141.
- 442 de Bélizal E, Lavigne F, Hadmoko DS, Degai JP, Dipayana GA, Mutagin BW, Marfai MA,
443 Coquet M, Le Mauff B, Robin AK, Vidal C, Cholik N, Aisyah N (2013) Rain-triggered
444 lahars following the 2010 eruption of Merapi volcano, Indonesia: A major risk. *Journal of*
445 *Volcanology and Geothermal Research* 261: 330-347.



- 446 Doyle EE, Cronin SJ, Cole SE, Thouret JC (2010) The coalescence and organization of
447 lahars at Semeru volcano, Indonesia. *Bulletin of Volcanology* 72(8): 961-970.
- 448 Dumaisnil C, Thouret JC, Chambon G, Doyle EE, Cronin SJ (2010) Hydraulic, physical
449 and rheological characteristics of rain-triggered lahars at Semeru volcano, Indonesia. *Earth
450 and Surface Processes and Landform* 35: 1573-1590.
- 451 Ferrer-Julio M, Estrela T, Sanchez del Corral Jimenez A, Garcia-Melendez E (2003)
452 Generation of a curve number map with continuous values based on saturated hydraulic
453 conductivity. XI World Water Congress, 5-9 October 2003, Madrid, Spain: 1-10.
454 <http://iwra.org/member/index.php?mainpage=&page=286&congressyear=2003>
- 455 Gentile F, Bisantino T, Puglisi S, Trisorio Liuzzi G (2006) Analysis and modeling of debris
456 flows in Gargano watersheds (Puglia region, Southern Italy). *WIT Transactions on Ecology
457 and the Environment* 90: 181-191.
- 458 Hawkins RH, Hjelmfelt AT, Zevenbergen AW (1985) Runoff probability storm depth and
459 curve numbers. *Journal of the Irrigation and Drainage Division* 111: 330-340.
- 460 Kean W, McCoy S, Tucker G, Staley D, Coe J (2013) Runoff-generated debris flows:
461 Observations and modeling of surge initiation, magnitude, and frequency. *Journal of
462 Geophysical Research: Earth Surface* 118: 1-18.
- 463 Keefer DK, Wilson RC, Mark RK, Brabb EE, Brown WM, Ellen SD, Harp EL, Wieczorek,
464 GF, Alger CS, Zatkan RS (1987) Real-time landslide warning during heavy rainfall.
465 *Science* 238(4829): 921-5.
- 466 Iverson RM (1997) The physics of debris flows: *Reviews of Geophysics* 35: 245-296.



- 467 Lavigne F, Thouret JC, Voight B, Suwa H, Sumaryono A (2000) Lahars at Merapi volcano,
468 Central Java: an overview. *Journal of Volcanology and Geothermal Research* 100: 423-456.
- 469 Lavigne F, Thouret JC (2002) Sediment transport and deposition by rain-triggered lahars at
470 Merapi Volcano, Central Java, Indonesia. *Geomorphology* 49: 45-69.
- 471 Llanes F, Ferrer PK, Gacusan R, Realino V, Obrique J, Eco RN, Lagmay AMF (2015)
472 Scenario-based maps using flo-2d and IFSAR-derived digital elevation models on the
473 November 2006 rainfall-induced lahars, Mayon Volcano, Philippines. *ACRS 2015*
474 *Proceedings, Asian Association on Remote Sensing.*
- 475 Marchi L, Arattano M, Deganutti A. (2002) Ten years of debris-flow monitoring in the
476 Moscardaro Torrent (Italian Alps), *Geomorphology* 46: 1–17, doi:10.1016/S0169-
477 555X(01)00162-3.
- 478 Mishra S K, Singh VP (2003) Soil conservation service curve number (SCS-CN)
479 methodology. Kluwer Academic Publishers, Dordrecht, Netherlands.
- 480 Natural Resource Conservation Services (2008) Rainfall-Frequency and Design Rainfall
481 Distribution for Selected Pacific Islands. Engineering Technical Note No. 3, United States
482 Department of Agriculture:115 pp.
- 483 O'Brien J, Julien P, Fullerton W (1993) Two-dimensional water flood and mudflow
484 simulation. *J. Hydraul. Eng.-ASCE* 119: 244-261.
- 485 Ortiz A. (2017) Modelado de conectividad y contribución de escorrentía superficial lateral
486 en la dinámica de flujos granulares de áreas volcánicas activas. PhD thesis, Universidad
487 Autónoma de San Luis Potosí, Facultad de Ciencias, México: 224 pp.



488 Ortiz-Rodríguez AJ, Borselli L, Sarocchi D (2017) Flow connectivity in active volcanic
489 áreas: use of index of connectivity in the assessment of lateral flow contribution to main
490 streams. *Catena* 157: 90 – 111.

491 Roverato M, Capra L, Sulpizio R, Norini G (2011) Stratigraphic reconstruction of two
492 debris avalanche deposits at Colima Volcano (Mexico): Insights into pre-failure conditions
493 and climate influence. *Journal of Volcanology and Geothermal Research* 207: 33-46.

494 Scott KM, Vallance JV, Kerle N, Macias JL, Strauch W, Devoli G (2005) Catastrophic
495 precipitation-triggered lahars at Casita Volcano, Nicaragua: occurrence, bulking and
496 transformation. *Earth Surface Processes and Landforms* 30: 59-79.

497 Sheridan MF, Connor CB, Connor L, Stinton AJ, Galacia O, Barrios G (2007) October
498 2005 Debris Flows at Panabaj, Guatemala: Hazard Assessment. American Geophysical
499 Union, Spring Meeting 2007, abstract #V33A-07.

500 Takahashi T (2007) Debris Flow: Mechanics Prediction, and Countermeasures. Taylor and
501 Francis/Balkema, Leiden: 448 pp.

502 Umbal JV, Rodolfo KS (1996) The 1991 lahars of southwestern Mount Pinatubo and
503 evolution of the lahar-dammed Mapanuepe lake. *Fire and mud; eruptions and lahars of*
504 *Mount Pinatubo, Philippines, P. I. o. V. a. Seismology, ed., Quezon, Philippines: pp. 951-*
505 *970.*

506 USDA-NRCS (U.S. Department of Agriculture-Natural Resources Conservation Service).
507 (2007) Hydrologic soil groups. National engineering handbook. Part 630 hydrology,
508 Washington, DC.



509 van Westen CJ, Daag AS (2005) Analysing the relation between rainfall characteristics and
510 lahar activity at Mount Pinatubo, Philippines. *Earth and Surface Processes and Landform*
511 30: 1663-1674.

512 Van Wyk Vries B, Kerle N, Petley D (2000) Sector collapse forming at Casita volcano,
513 Nicaragua. *Geology* 28(2): 167-170.

514 Vázquez R, Suriñach E, Capra L, Arámbula-Mendoza R, Reyes-Dávila G (2016a) Seismic
515 characterisation of lahars at Volcán de Colima, Mexico. *Bulletin of Volcanology* 78: 8.

516 Vázquez R, Capra L, Coviello V (2016b) Factors controlling erosion/deposition
517 phenomena related to lahars at Volcán de Colima, Mexico. *Natural Hazards and Earth*
518 *System Sciences* 16: 1881–1895.

519 Zanuttigh B, Lamberti A (2007) Instability and surge development in debris flows. *Rev.*
520 *Geophys.* 45: RG3006, doi:10.1029/2005RG000175.

521 Zobin VM, Placencia I, Reyes G, Navarro C (2009) The characteristics of seismic signal
522 produced by lahars and pyroclastic flows: Volcán de Colima, Mexico. *Journal of*
523 *Volcanology and Geothermal Research* 179: 157-167.

524



525 **Figure captions**

526 Figure 1. a) Aster image (4, 5 and 7 bands in RGB combination) where main watersheds at
527 Volcán de Colima are represented. The locations of the monitoring stations are indicated.
528 The inset show the location of the raingauge of the Meteorological National Service at the
529 summit of the Nevado de Colima Volcano.

530 Figure 2. a) Panoramic view of the Volcán de Colima showing the unvegetated main cone
531 mostly composed by loose volcanic fragments. b) Montegrande and c) La Lumbre ravines
532 in the middle reach where it is possible to observe the main channel flanked by 10-15m-
533 high terraces mainly constituted by debris avalanche deposits.

534 Figure 3. a) Cumulative and b) normalized values of rainfall of hurricanes Jova, Manuel
535 and Patricia calculated at 10 min-intervals. c) Normalized curve of total rainfalls cumulated
536 at 15, 30, 60 minutes and 1, 3, 6, 12, 18, 24, 28 hrs. Dotted line represents the average value
537 between Manuel and Patricia hurricanes.

538 Figure 4. a) Seismic record of the lahar triggered during the Hurricane Jova, on 12 October,
539 2011. b) Seismic record of the lahar triggered during the 11 June, 2013 events. Main pulses
540 are indicated with roman letters. c) Images captures by the camera corresponding to the
541 main lahar pulses as indicated in figure b.

542 Figure 5. Images showing the morphology of the channel at the monitoring site of the
543 Montegrande ravine, a) the day before and b) the day after the Hurricane Jova. c)
544 Topographic profiles showing that the channel was eroded 1.5 m in depth.



545 Figure 6. Seismic record of the lahar triggered during the Hurricane Manuel, on 15
546 September, 2013, recorded along the Montegrande ravine

547 Figure 7. a) Seismic record of the lahar triggered during the Hurricane Patricia, on 26
548 October, 2015, recorded along the La Lumbre ravine. Main lahar pulses are indicated with
549 roman letters. b) Images captured by the camera corresponding to the main pulses as
550 indicated in figure a.

551 Figure 8. Diagrams showing the main lahar pulses (red triangles) as detected from the
552 seismic signal of the analyzed events in relation with the accumulated rainfall (dark line),
553 rainfall intensity (10m/hr) (gray line) and simulated watershed discharge (blue line) for the
554 following hidrometeorological events a) Jova; b) Manuel; c) 13 June, 2013; and d) Patricia.

555 Table 1. Data collected for the events here studied.
556

557 Table 2. Normalized accumulated rains (in percentage) at progressive time steps.

558



559 Table 1. Data collected for the events here studied.

Event	ravine	Seismic record	Image record	Total rain (mm)	Max. rain intensity (mm/hr)
Jova	Montegrande			240	43
Manuel	Montegrande	X		300	32
Patricia	Lumbre	X	X	400	37
11 June 2013	Montegrande	X	X	120	140

560

561



562 Table 2. Normalized accumulated rains (in percentage) at progressive time steps.

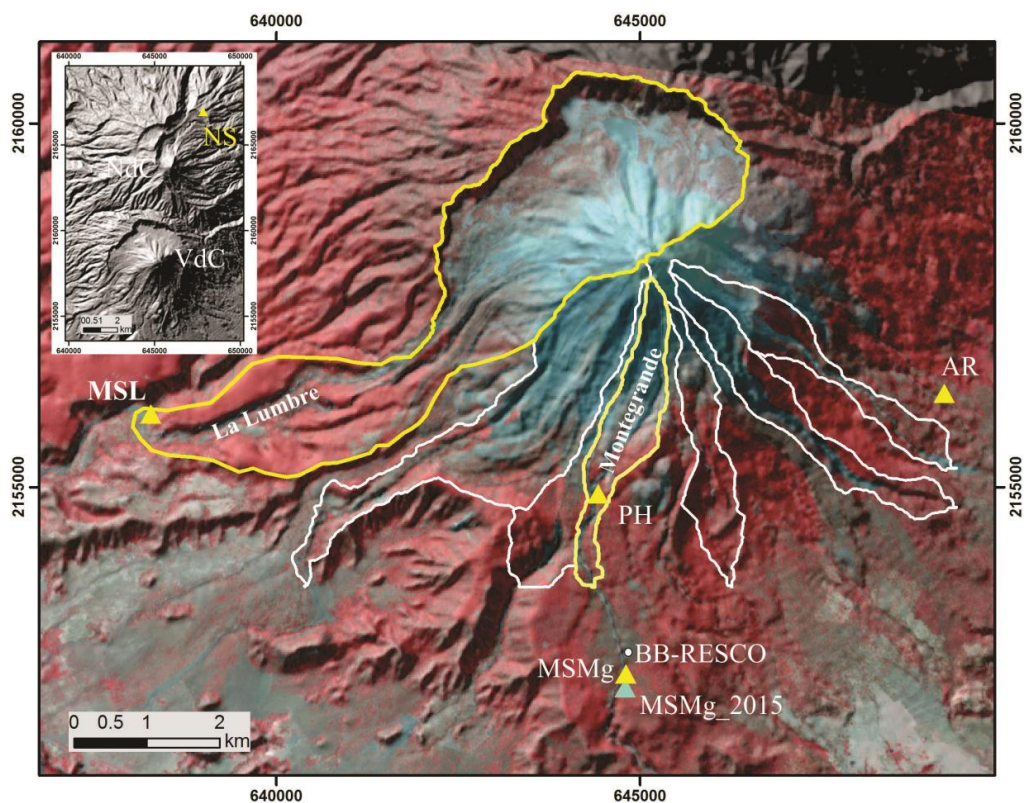
Event/time (hrs)	0.25	0.5	1	2	3	6	12	24	27
Jova	0.0011	0.0016	0.0035	0.0172	0.0329	0.1411	0.7073	0.968	0.9943
Manuel	0.0023	0.0035	0.0042	0.0072	0.0151	0.0341	0.1548	0.735	0.9181
Patricia	0.0002	0.0004	0.0009	0.0062	0.0174	0.0556	0.2544	0.829	0.9782
average	0.00125	0.00195	0.00255	0.0067	0.01625	0.04485	0.2046	0.782	0.9481

563 The average values refer to hurricanes Manuel and Patricia.

564



565 Fig. 01

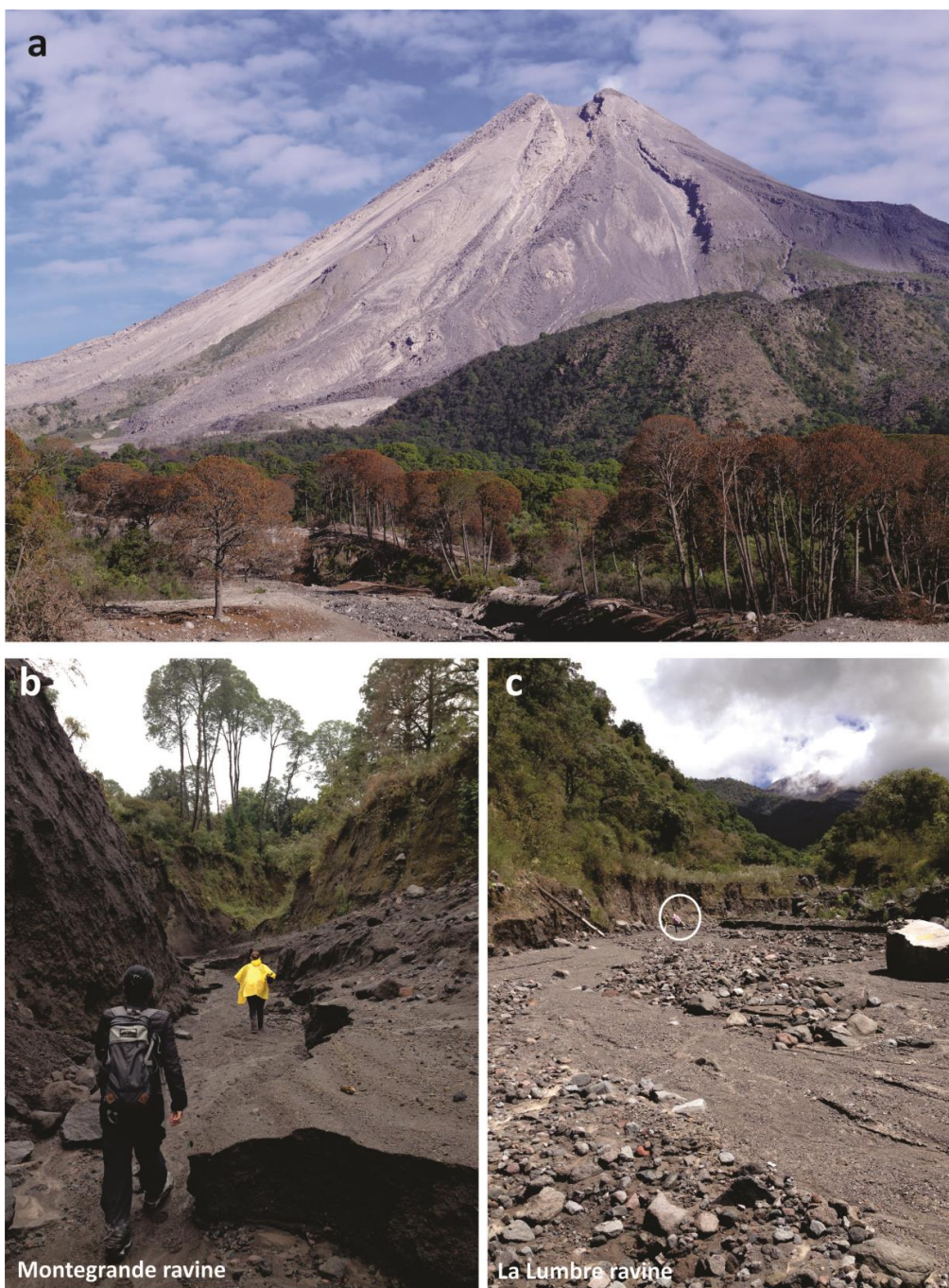


566

567



568 Fig. 02



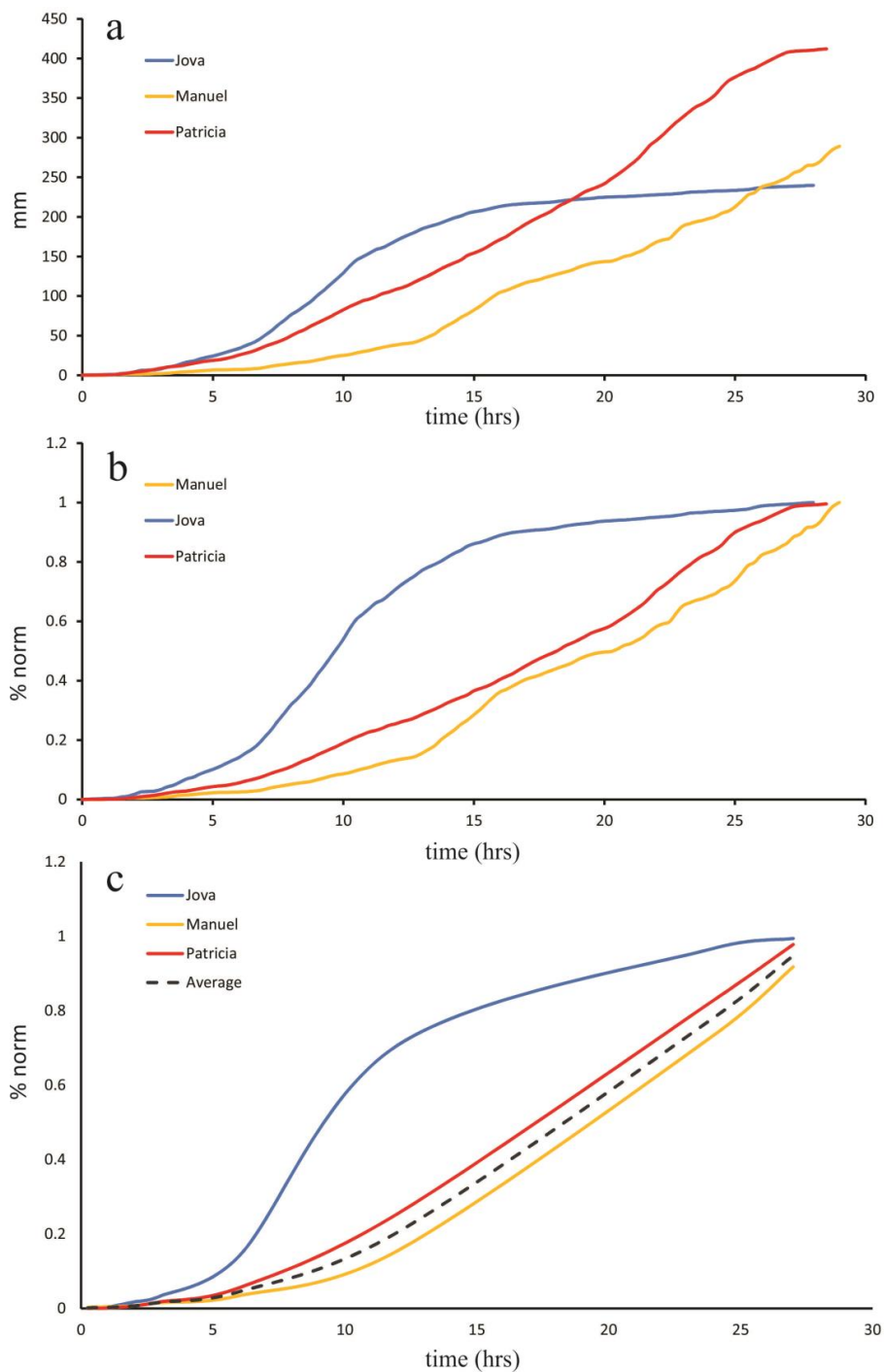
569

570



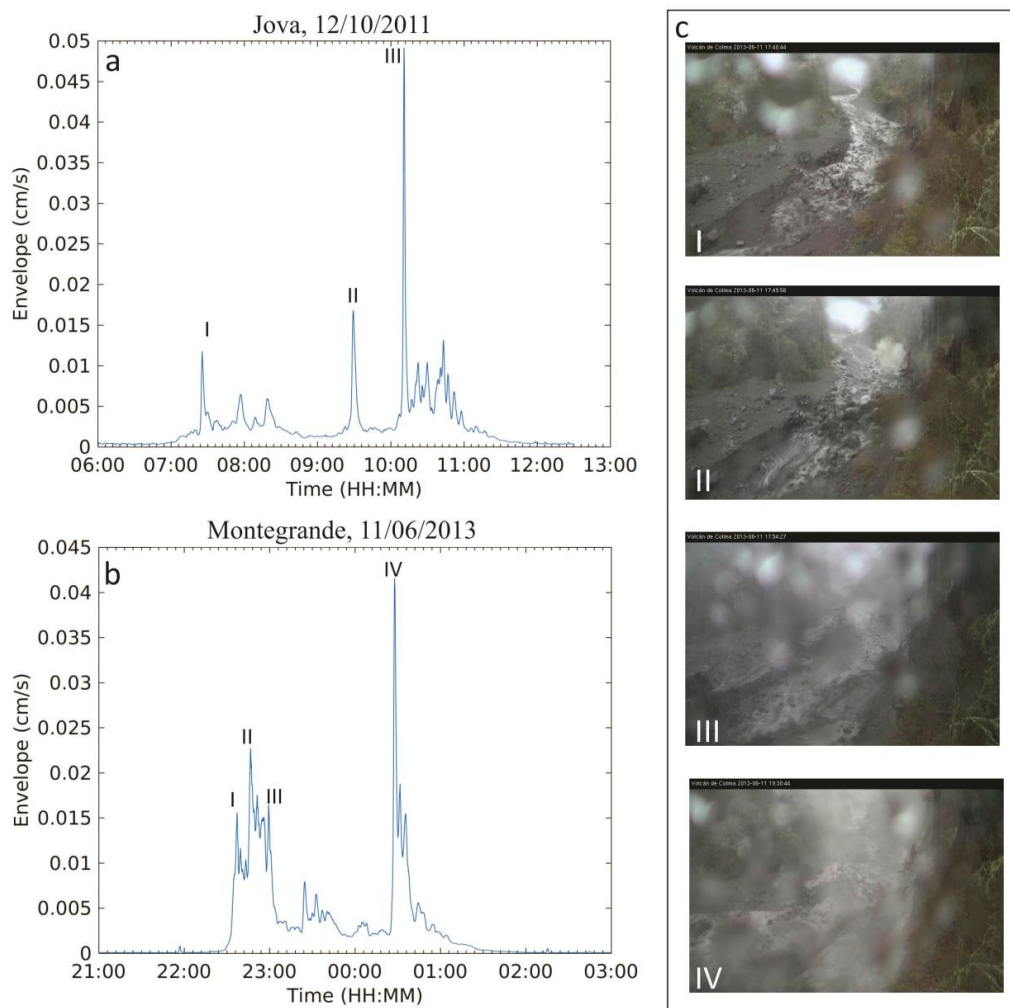
571 Fig-03

572





573 Fig. 04

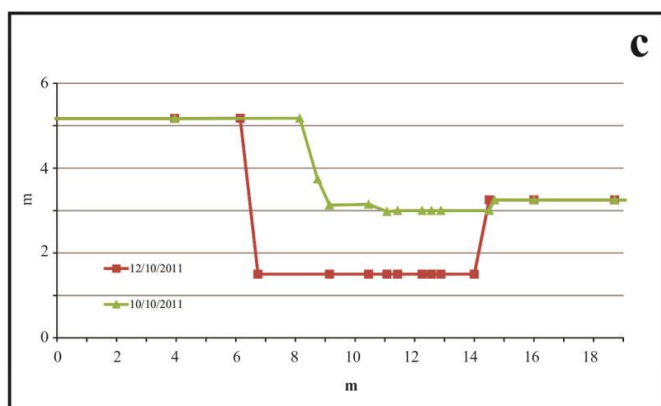


574

575

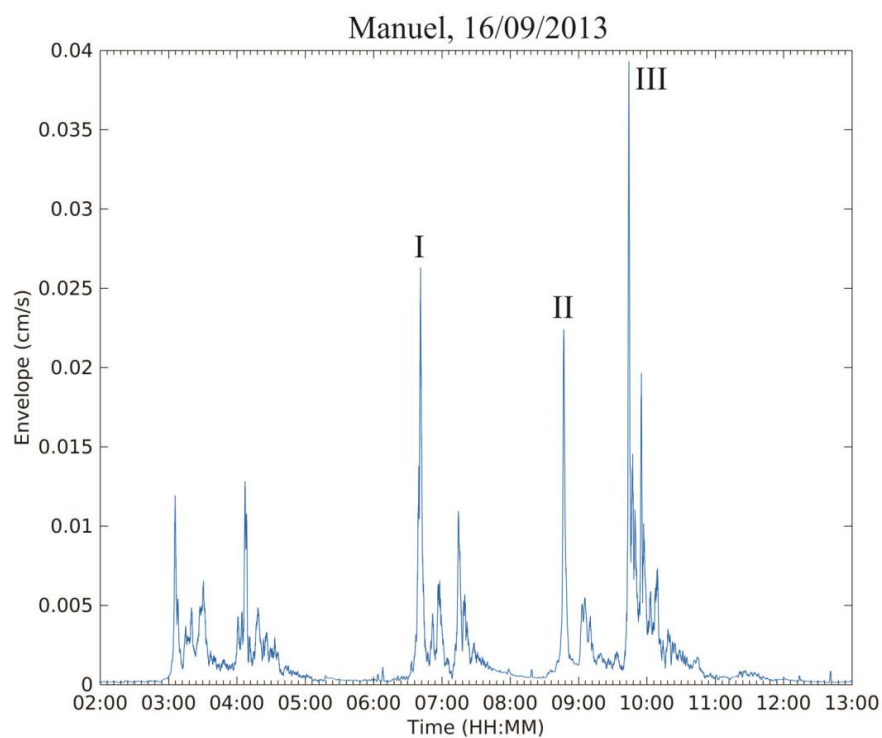


576 Fig. 05





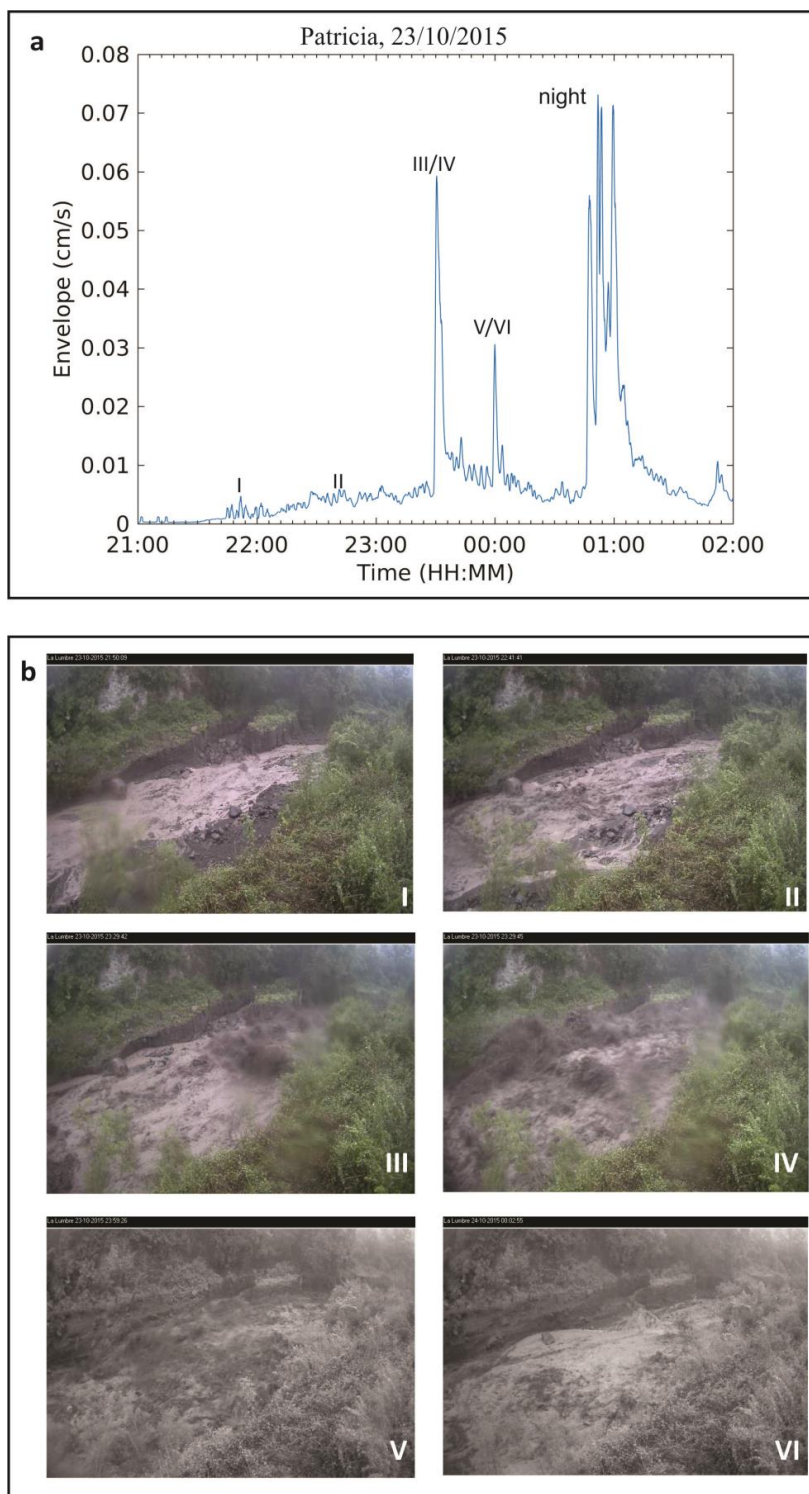
577 Fig. 06



578

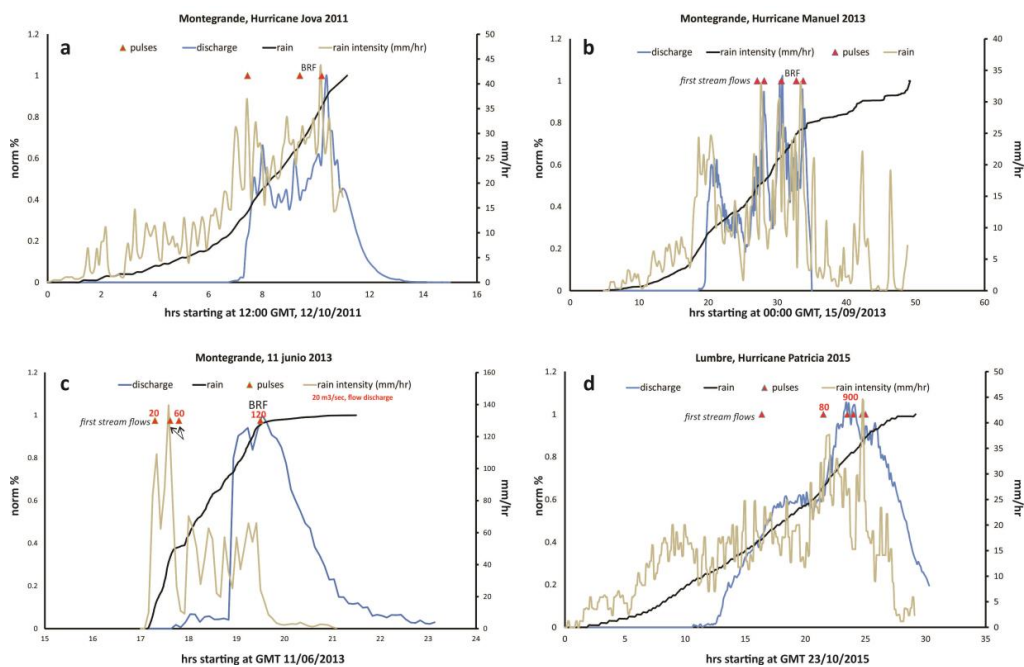


579 Fig. 07





580 Fig. 08



581

582